INT. J. REMOTE SENSING, 1999, VOL. 20, NO. 17, 3333–3344

Reducing the effects of space-varying, wavelength-dependent scattering in multispectral imagery

M. J. CARLOTTO†

Pacific-Sierra Research Corp., 1400 Key Blvd, Suite 700, Arlington, Virginia 22209, USA

(*Received 3 January 1996; in revised form 25 May 1998*)

Abstract. A new method for reducing the effects of space-varying, wavelength-dependent scattering in multispectral imagery caused by smoke and haze is described. It is intended for use in situations where atmospheric scattering affects the shorter wavelengths and varies in space. The method converts an image in which space-varying scattering is present into an image where the scattering has been equalized over the entire image, so that previously developed techniques for removing constant scattering effects can be used. The spectral measurement space is viewed as consisting of two subspaces: one spanned by the bands that are affected by scattering, the other by the bands that are not. A correspondence between the two subspaces is established and used to predict the values of the former bands (i.e., what their values would be without scattering) from the latter. Our haze equalization algorithm is compared to an earlier de-hazing algorithm developed by Lavreau that subtracts a portion of the fourth tasselled cap feature, used as an estimate of the atmospheric component, from the visible bands. While both are shown to be effective in removing space-varying smoke and haze, the de-hazing algorithm tends to remove subtle detail and increases the spectral correlation between the visible bands, while the haze-equalization algorithm preserves subtle detail and maintains the spectral balance between bands.

1. Introduction

Atmospheric scattering affects the ability to accurately estimate physical properties of the surface (e.g., soil moisture and biomass) from remotely sensed imagery. In many cases this can, in turn, reduce the accuracy of land cover classification and change detection algorithms. Although a variety of atmospheric correction techniques have been described, few are capable of handling space-varying effects, e.g., smoke plumes from brush fires and factories, smoke and haze that is present in and around urban areas, and haze that often settles in low-lying areas overnight. It has been observed that the fourth tasselled cap feature is particularly sensitive to the amount of aerosols in the atmosphere (Crist et al 1986). Lavreau (1991) describes one such method for removing space-varying haze and smoke that subtracts a portion of the fourth tasselled cap feature from those spectral bands requiring correction.

†Correspondence address: 5 Ryan Place, Beverly, Massachusetts 01915, USA; e-mail: markc@psrw.com

International Journal of Remote Sensing
ISSN 0143-1161 print/ISSN 1366-5901 online
http://www.tandf.co.uk/JNLS/res.htm
http://www.taylorandfrancis.com/JNLS/res.htm

A new method for reducing the effects of space-varying, wavelength-dependent scattering in multispectral imagery caused by smoke and haze is described in this paper. It is intended for use in situations where atmospheric scattering affects the shorter wavelengths and varies in space. In our approach the spectral measurement space is viewed as consisting of two subspaces: one spanned by the bands affected by scattering, the other by the bands that are not. The correspondence between the two subspaces is used to predict the former bands as a function of the latter on a pixel-by-pixel basis. Our method converts an image in which space-varying scattering is present into an image where the scattering has, in effect, been equalized over the entire image so that previously developed techniques for removing constant scattering effects can be used.

2. Background

Assume the atmosphere can be modelled as a horizontally homogeneous medium, the earth is a Lambertian reflector, and atmospheric properties which vary exponentially with altitude can be assumed to be constant over the scene (Sjoberg and Horn 1983). We also assume that the contribution of the ambient illumination (skylight) can be neglected. Under these conditions, the sensed irradiance (brightness) z can be modelled by a linear relation

$$z = ar + b \tag{1}$$

where r is the radiance of the surface, a represents the effects of atmospheric transmittance, sensor gain, and other multiplicative factors, and b represents the contribution of the path radiance. When the scattering is constant over the image,

$$z(i,j) = ar(i,j) + b \tag{2}$$

The brightness values at two or more pixels in the image together with measurements of the surface radiance at the corresponding locations on the ground can be used to solve for a and b.

When ground data is not available several methods have been developed to estimate the path radiance component. Dark pixel subtraction (Crane 1971) assumes that somewhere in the image there is a pixel with zero illumination or zero reflectivity such that the sensor irradiance depends only on the path radiance. The regression method (Potter and Mendlowitz 1975) and regression intersection method (Crippen 1987) have been developed for multispectral images. The former obtains an estimate of the path radiance contributions by performing a linear regression analysis between two bands at a time over pixels with the same material type. The latter performs linear regression analyses over two or more sets of pixels each with the same material type and uses the intersection of the regression lines to estimate the path radiance terms.

All of the above methods assume that the effects of scattering are constant over the image. A de-hazing technique for Landsat Thematic Mapper (TM) developed by Lavreau (1991) subtracts a portion of the fourth tasselled cap feature (Crist and Cicone 1984) from each band. The method effectively removes space-varying haze but causes the corrected bands to become more correlated thus altering the spectral balance of the data.

3. Methodology

When the effects of scattering are not constant over the image, the image formation model becomes

$$z(i,j)=a(i,j)r(i,j)+b(i,j) \tag{3}$$

Assume that it is possible to segment the image into disjoint regions within which the radiance of the surface can be assumed to be constant. Let S_k represent the set of pixels in the k-th region. Within the k-th region the brightness is

$$z_{k'}=a_{k'}r_k+b_{k'} \tag{4}$$

where r_k is the surface radiance. The terms $a_{k'}$ and $b_{k'}$, $k' \in S_k$ represent the effective variation in the atmospheric transmittance and path radiance for the pixels within the region. The mean value of the brightness in the k-th region is

$$\hat{z}_k=E[z_{k'}]=E[a_{k'}]r_k+E[b_{k'}] \tag{5}$$

and is computed over the pixels $k' \in S_k$. We assume that the pixels within each of the K regions are randomly distributed throughout the image and that the variation in scattering within the image is such that the distribution of atmospheric transmittance and path radiance effects is the same in all regions. The validity of this assumption is examined in §5. Thus $E[a_{k'}]=\mu_a=a$ and $E[b_{k'}]=\mu_b=b$ are the same for all of the regions and

$$\hat{z}_k=ar_k+b \tag{6}$$

Assembling the K regions back into an image we have

$$\hat{z}(i,j)=ar(i,j)+b \tag{7}$$

thus reducing the space-varying case to a simpler one in which the scattering can be treated as a constant over the image (equation (2)). Our method converts an image in which space-varying scattering is present into an image where the scattering has, in effect, been equalized over the entire image so that previously developed techniques for removing constant scattering effects can be used. A key requirement is that we are able to segment the image into regions of constant surface radiance.

The dependence of scattering on wavelength is a function of the size of the particles relative to the wavelength of the radiation (Schanda 1986). Scattering by molecules whose radius is much less than the wavelength of light λ has a λ^4 dependence, affecting the shorter wavelengths below 0.4 μm. Particulates such as smoke and haze with a radius between 0.1λ and 10λ have a wavelength dependence between λ^{-4} and λ^0, respectively. Depending on the amount of smoke and haze in the atmosphere, portions of the surface obscured in the shorter wavelengths may be visible in the infrared. As the size of the particles increases relative to λ the scattering does not depend strongly on wavelength. Thick clouds, fog, and dust thus tend to be opaque in the visible and the infrared portions of the spectrum.

In multispectral imagery, haze (and smoke) tend to affect the shorter wavelengths (i.e., the visible bands), often having negligible effect in the infrared bands. Let the multispectral image be divided into two sets of bands $Z=\{X, Y\}$ where X are the bands that are affected by haze and Y are the bands that are not. To be specific we shall focus on Landsat TM (although the method is applicable to other multispectral sensors as well) and assume that in a given situation the visible bands (Landsat TM bands 1-3) are affected by haze while the infrared bands (Landsat TM bands 4, 5

and 7) are not. The validity of this assumption is also examined in §5. Thus $x(i, j, m)$ is the brightness at pixel (i, j) in the m-th visible band and $y(i, j, n)$ is the brightness at pixel (i, j) in the n-th infrared band.

Let X^M and Y^N denote the corresponding M- and N-dimensional visible and infrared subspaces where $M = N = 3$. A point in the infrared subspace corresponds to pixels that have the same values in the infrared bands. It is conjectured that pixels with the same infrared values are likely to be the same surface material with the same illumination and topography. In the absence of scattering, each point in the infrared subspace is assumed to correspond to a point in the visible subspace (figure 1(*a*)). This is an approximation because the visible bands provide information not contained in the infrared. If we assume that the distribution of pixels with the same infrared values are randomly distributed throughout the image, when scattering is present the visible band values of those pixels will be affected by varying amounts, i.e., will have higher or lower brightness values because of increased or decreased path radiance in different parts of the image. Thus in situations where space-varying scattering is present in the visible bands, points in the infrared subspace will correspond to a set of points in the visible subspace (figure 1(*b*)).

Figure 2 shows two coregistered Landsat TM band 1 images over Bitterfeld Germany. The images are $955 \times 807 = 770\,685$ pixels in size. The image shown in figure 2(*a*) was acquired in September 1986 and contains a great deal more smoke and haze than the second image (*b*) which was acquired about one year later. Analysis of bands 4, 5 and 7 in the September 1986 image reveal that there are over 81 000 regions, i.e, unique combinations of band 4–5–7 values. The locations of pixels contained in one particular combination are plotted as crosses in (*a*) and (*b*). This particular combination of pixel values occurs over forested areas which showed little if any change between the two acquisitions. Histograms of band 1 values at those locations in the two images are plotted in (*c*) and (*d*). In comparing the two histograms, (*c*) has a higher mean and standard deviation than (*d*) because there is more smoke and haze in (*a*) than in (*b*).

The correspondence between the two subspaces is used to establish a functional relationship that is used, in turn, to predict the values of the visible bands (i.e., what their values would be without scattering) as a function of the infrared bands. Let $\mathbf{y}_k = \{y_k(n)\}$ denote the vector corresponding to the k-th unique combination of values in the infrared bands where $y_k(n)$ is the value of the n-th infrared band for the k-th combination (region). Let $\{\mathbf{x}_{k'}, k' \in S_k\}$ denote the set of visible band values that occur within the k-th region where $\mathbf{x}_{k'}(m)$ is the value of pixel k' in the m-th band.

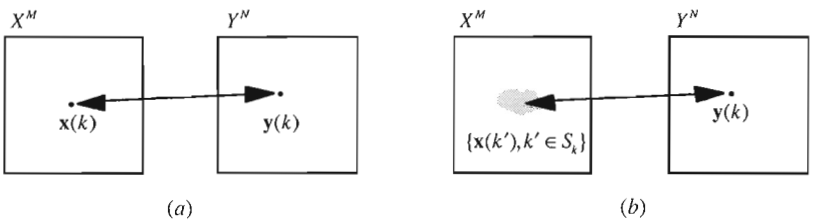

Figure 1. Idealized relation between subspaces with and without haze. (*a*) In the absence of scattering, each point in the infrared subspace corresponds to a point in the visible subspace. (*b*) When scattering is present n the visible bands, each point in the infrared subspace corresponds to multiple points in the visible subspace.

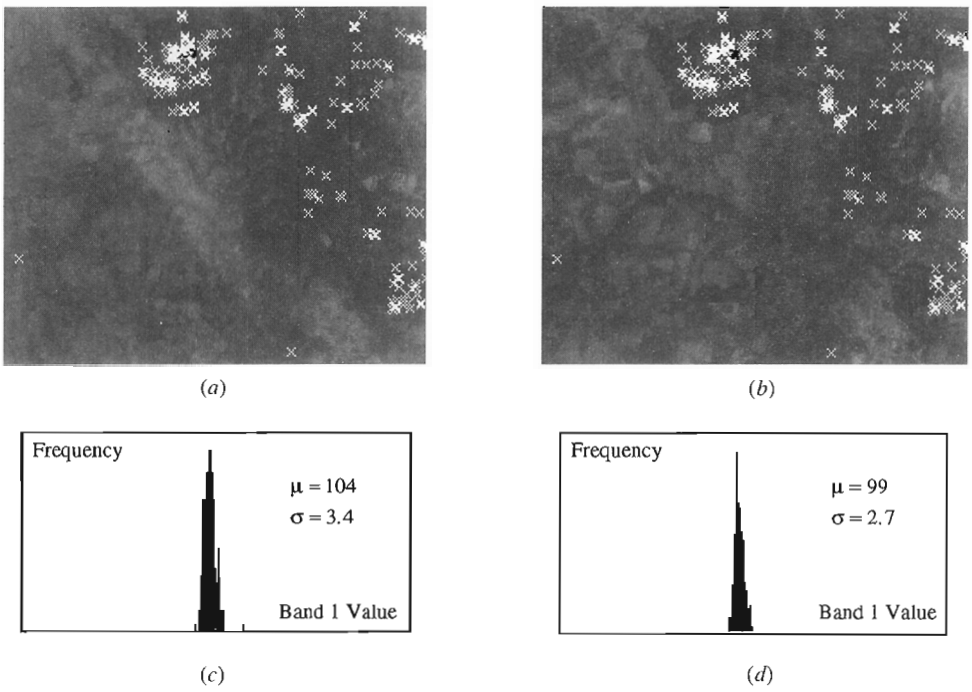

Figure 2. Example showing effects of haze in Landsat TM visible band over Bitterfeld, Germany. (*a*) Band 1 of September 1996 image. Locations of pixels having the same infrared values in bands 4, 5 and 7 marked by crosses. (*b*) Band 1 of September 1987 image. Locations are the same as in September 1986 image. (*c*) Histogram of September 1986 band 1 image computed over locations marked by crosses. (*d*) Histogram of September 1987 band 1 image computed over locations marked by crosses.

The joint distribution

$$P(x(m), \mathbf{y}) = P(x(m), y(1) \ldots y(N)) \tag{8}$$

is the probability of observing a particular combination of values in the m-th visible band and all N infrared bands. For a given combination of values in the infrared bands, the optimal estimate for the value of the m-th visible band is given by the conditional mean:

$$\hat{x}_k(m) = E[x_{k'}(m) | \mathbf{y}_k] = \frac{\sum_{k' \in S_k} x_{k'}(m) P(x(m) = x_{k'}(m), \mathbf{y} = \mathbf{y}_k)}{P(\mathbf{y} = \mathbf{y}_k)} \tag{9}$$

It can be shown that the conditional mean minimizes the mean-squared prediction error of $x(m)$ as a function of $\mathbf{y}$ (Papoulis 1965). In other words it provides the best single haze-free value to assign to the $x_{k'}(m)$ in each region.

The above computation can be efficiently performed using two tables G and H_m containing K entries each. In the first table, $G = \{g[\mathbf{y}_k]\}$, we count the number of times each $\mathbf{y}_k$ combination occurs, i.e., the number of pixels in the image where $\mathbf{y} = \mathbf{y}_k$ and store it in the k-th entry. In the second table $H_m = \{h_m[\mathbf{y}_k]\}$ we add the values in the m-th visible band that occur for each $\mathbf{y}_k$ combination and store it in

the k-th entry; i.e.,

$$h_m[\mathbf{y}_k] = \sum_{k' \in S_k} x_{k'}(m) \tag{10}$$

The haze-equalization then becomes a simple table look-up

$$\hat{x}(i, j, m) = \frac{h_m[\mathbf{y}(i, j)]}{g[\mathbf{y}(i, j)]} \tag{11}$$

and is equivalent to the result given in equation (9). The above procedure is repeated for each of the M visible bands requiring equalization.

4. Experimental results

The above method has been evaluated on several images to date. We present results from one of these images over Bitterfeld, Germany shown previously in figure 2. Figure 3 shows the original and haze-equalized band 1-3 images for the September 1986 image. The results have been stretched for visual presentation. Like the de-hazing technique described by Lavreau (1991), our method effectively removes the space-varying haze. Lavreau's de-hazing algorithm subtracts a portion of the fourth tasselled cap feature $t(i, j)$ from the visible bands

$$\hat{x}(i, j, m) = x(i, j, m) - [t(i, j) - t_0]c(m) \tag{12}$$

where t_0 is a haze threshold and $c(m)$ are empirically derived parameters. (We used a haze threshold $t_0 = 8$ and the values for $c(m)$ given in Lavreau (1991) for the Bitterfeld image.) As noted by Crist *et al.* (1986) the fourth tasselled cap feature responds to atmospheric haze as well as to senescent vegetation, man-made materials (e.g., roads), some soils and water. Thus by subtracting a portion of the fourth tasselled cap feature from the visible bands, information about the surface may be lost in the process of removing the haze. One such example is shown in figure 4 in which road information lost by de-hazing has been retained by haze equalization.

As noted by Lavreau (1991), de-hazing can increase the correlation between bands. Stated another way, de-hazing alters the covariance between spectral bands. Table 1 gives the mean vector and covariance matrix for bands 1-5 and 7 of the original September 1986 image (a), our haze equalized image (b), and Lavreau's de-hazed image (c). The mean and covariance of the haze equalized image are similar to those of the original image. On the other hand, there are significant differences between the original and de-hazed images.

The eigenvalues describe the spectral covariance structure of a multispectral image. Figure 5(*a*) compares the distribution of the eigenvalues corresponding to the three eigenvectors (principal components) computed from bands 1-3 before and after application of Lavreau's algorithm. A significant increase in the first eigenvalue indicates an increase in the spectral covariance between the three visible bands. Figure 5(*b*) compares the distribution of the eigenvalues before and after application of our haze equalization algorithm. The covariance structure of the haze equalized bands is similar to the original (uncorrected) bands. This is also seen in figure 5(*c*) and (*d*) which compare distributions of eigenvalues corresponding to all six eigenvectors computed from the visible and infrared bands (thermal band excluded). These plots show that the haze equalization algorithm better preserves the overall covariance structure and spectral balance of the multispectral image than de-hazing.

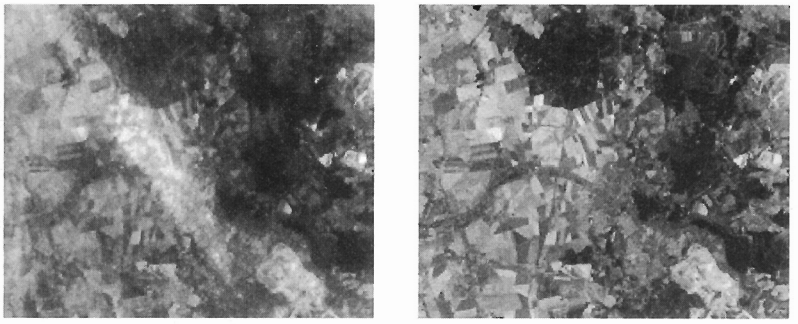

(*a*) Band 1 original (left) and corrected (right)

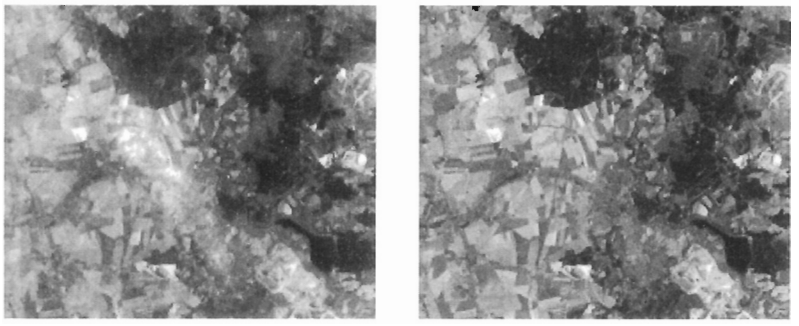

(*b*) Band 2 original (left) and corrected (right)

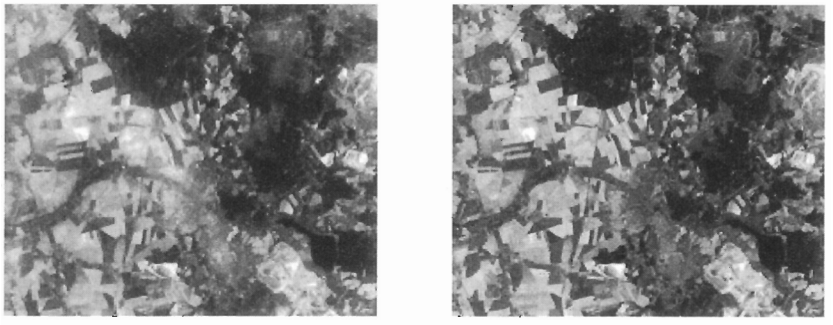

(*c*) Band 3 original (left) and corrected (right)

Figure 3. Haze equalization results for Bitterfeld image. (*a*) Band 1, (*b*) band 2 and (*c*) band 3. Original images are on the left and the corrected images on the right.

5. Discussion

We have assumed that the image has been accurately segmented into regions of constant surface radiance and that the distribution of scattering effects is the same in all regions. The mean brightness of the m-th visible band in the k-th region

$$\hat{x}_k(m) = E[x_{k'}(m)] = E[a_{k'}(m)]r_k(m) + E[b_{k'}(m)] \tag{13}$$

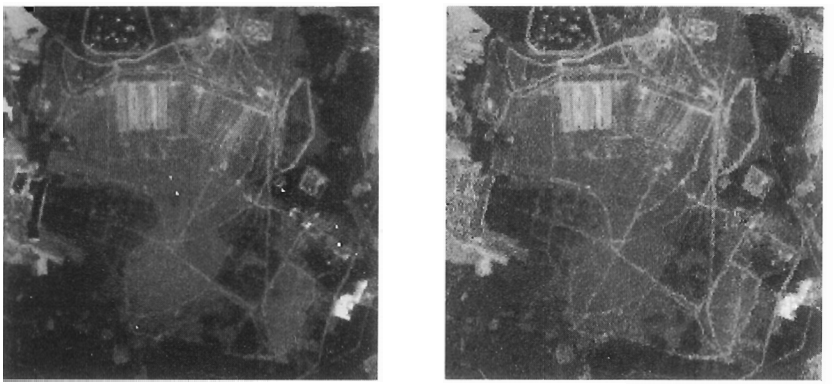

(*a*) (*b*)

Figure 4. Visual comparison of algorithms for band 1 over a portion of the Bitterfeld image. (*a*) De-haze algorithm, (*b*) haze-equalization algorithm.

Table 1. Multispectral mean vectors and covariance matrices for original, haze-equalized, and de-hazed images.

(a) Original					
116.066284	45.554211	50.109211	69.625824	71.849411	31.888096
127.000114	59.302757	103.847336	0.033049	160.567062	126.271233
59.302757	39.833733	62.917965	7.886708	110.276688	81.478416
103.847336	62.917965	123.433228	−20.487764	210.688232	165.396027
0.033049	7.886708	−20.487764	323.857666	71.057640	−44.248352
160.567062	110.276688	210.688232	71.057640	542.554688	344.827271
126.271233	81.478416	165.396027	−44.248352	344.827271	273.400940
(b) Haze-equalized					
115.600853	45.105686	49.666210	69.625824	71.849411	31.888096
97.215675	46.591694	86.843170	1.161113	162.753220	126.954926
46.591694	34.113445	55.777279	8.188755	110.966141	81.929604
86.843170	55.777279	111.220657	−21.229876	210.821304	165.665787
1.161113	8.188755	−21.229876	323.857666	71.057640	−44.248352
162.753220	110.966141	210.821304	71.057640	542.554688	344.827271
126.954926	81.929604	165.665787	−44.248352	344.827271	273.400940
(c) De-hazed					
56.208080	16.963457	17.564022	42.382725	29.187757	12.252388
201.142242	114.881042	188.957840	30.445232	307.457520	192.445755
114.881042	69.460320	110.166336	27.281473	182.937408	111.103218
188.957840	110.166336	186.410583	9.111508	300.428864	193.511002
30.445232	27.281473	9.111508	316.975281	89.896416	−26.092583
307.457520	182.937408	300.428864	89.896416	601.640198	340.576141
192.445755	111.103218	193.511002	−26.092583	340.576141	239.631714

is estimated from the infrared bands (equations (9), (11)). Assuming the surface radiance is constant and the atmospheric transmittance and the path radiance effects are the same in all regions,

$$E[x_k(m)] = \mu_a(m) r_k(m) + \mu_b(m) \tag{14}$$

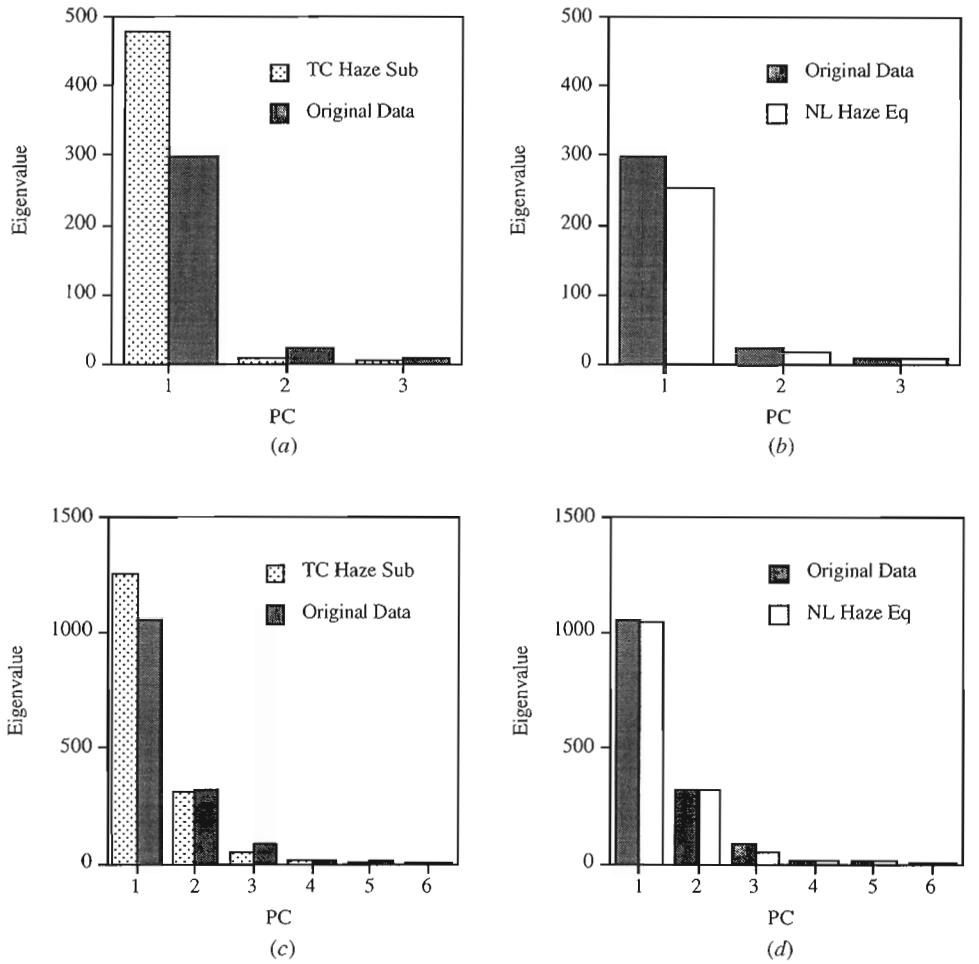

Figure 5. Covariance structure of multispectral image before/after de-hazing and haze equalization (*a*) Eigenvalues (visible bands) before/after de-hazing, (*b*) eigenvalues (visible bands) before/after haze-equalization (*c*) eigenvalues (all bands) before/after de-hazing, (*d*) eigenvalues (all bands) before/after haze-equalization.

In the absence of scattering, $\mu_a(m)=1$, $\mu_b(m)=0$, and $E[x_{k'}(m)]=r_k(m)$. The variance of the m-th visible band in the k-th region is

$$\mathrm{Var}[x_{k'}(m)]=r_k^2(m)\mathrm{Var}[a_{k'}(m)]+\mathrm{Var}[b_{k'}(m)]+r_k(m)\mathrm{Cov}[a_k(m),\, b_{k'}(m)] \quad (15)$$

where $\mathrm{Cov}[a_{k'}(m),\, b_{k'}(m)]$ is the covariance between the atmospheric transmittance and the path radiance. Given the same assumptions

$$\mathrm{Var}[x_{k'}(m)]=r_k^2(m)\sigma_a^2(m)+\sigma_b^2(m)+r_k(m)\sigma_{ab}^2(m) \quad (16)$$

In the absence of scattering, $\mathrm{Var}[x_{k'}(m)]=0$ otherwise, when scattering is present, the variance is a function of the surface radiance.

Figure 6 plots the mean value and standard deviation within regions greater than 100 pixels in size for bands 1–3 in the September 1986 image (the means are shown above the standard deviations). The results have been sorted in increasing order of

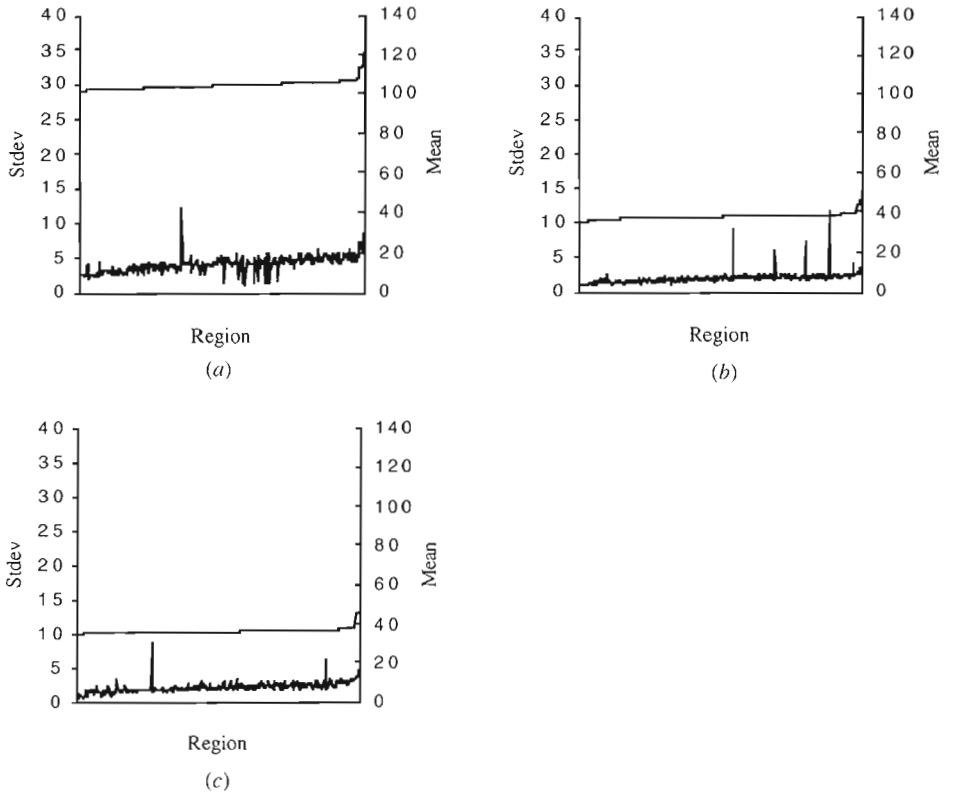

Figure 6. Mean and standard deviation within regions in image of Bitterfeld with more haze. (*a*) Within band 1, (*b*) within band 2, (*c*) within band 3.

the means. In all three, the standard deviation increases with the mean. The rate at which the standard deviation increases (i.e., the slope of the plot) is greater in band 1 than bands 2 and 3. The minimum value of the standard deviation is also greater in band 1 than bands 2 and 3. Although we do not know the actual values of the terms on the right-hand sides of equations (14) and (16), if our assumptions are valid the results in figure 6 can be interpreted as follows:

- The rate at which the standard deviation increases is related to variance of the atmospheric transmittance term $\sigma_a^2(m)$ in equation (16) which decreases with increasing wavelength.
- The minimum value of the standard deviation is related to the variance of the path radiance term $\sigma_b^2(m)$ in equation (16) which also decreases with increasing wavelength.

If our assumptions are valid, in an image with lesser amounts of space-varying scattering, the standard deviation should not increase as much and the minimum values of the standard deviation should be about the same in all bands. For comparison purposes we used bands 4, 5 and 7 from the September 1986 image to segment the September 1987 image. Because the two images were acquired a year apart there are regions in the September 1987 visible bands in which the surface radiance is not constant. Figure 7 plots the mean and standard deviation for bands 1–3 of the 1987

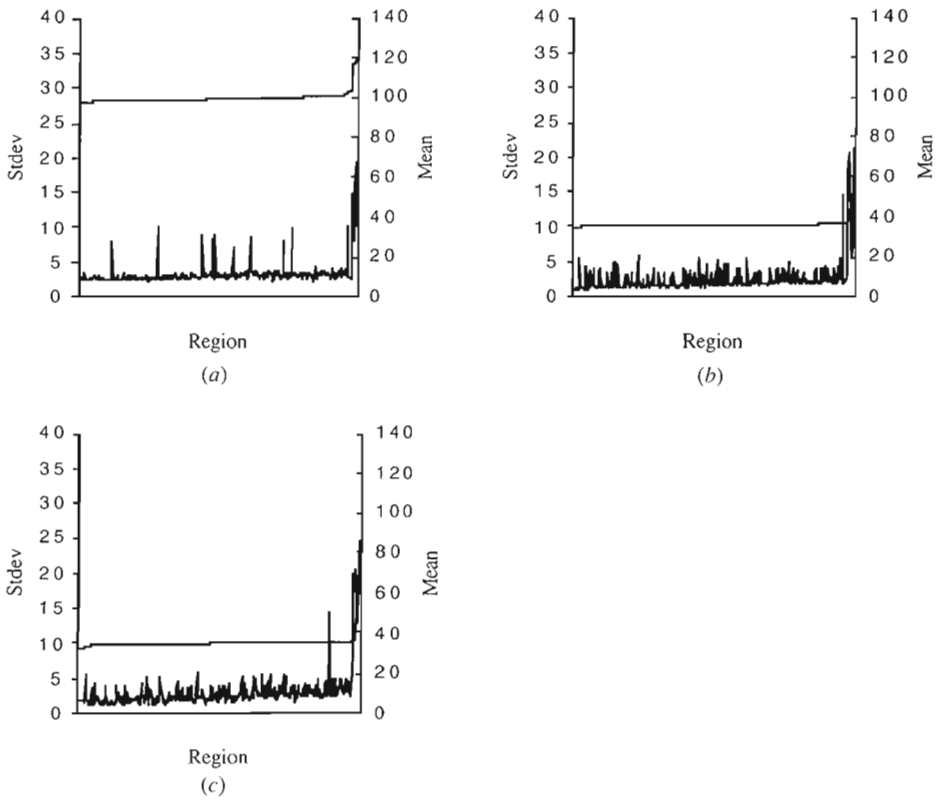

Figure 7. Mean and standard deviation within regions in image of Bitterfeld with less haze. (*a*) Within band 1, (*b*) within band 2, (*c*) within band 3.

image over regions with the same infrared values in the September 1986 image. The standard deviations are about the same overall and do not appear to increase as a function of the mean as in the 1986 image. The jump in the standard deviation at the far right in each plot in figure 7 occurs in the brightest regions which showed the greatest amount of change between the two dates.

The above assumes that scattering does not affect the infrared bands. But as noted earlier clouds, fog, and dust are opaque in the visible and infrared. At present we rely on the user to determine if the method is applicable to a given image. When it is applied to images containing clouds we have found that although the overall spectral balance is not altered, information about certain surface features is lost. For example, thin roads may disappear and the contrast of man-made objects within built up areas may be reduced. The development of more automated methods for determining when and where in an image to apply the technique is an area for future work.

5. Conclusion

A new method for reducing the effects of space-varying, wavelength-dependent scattering in multispectral imagery caused by smoke and haze was described. The method converts an image in which space-varying scattering is present into an image where the scattering has, in effect, been equalized over the entire image so that

previously developed techniques for removing constant scattering effects can be used. The algorithm predicts the values of those bands that are affected by scattering from those that are not on a pixel-by-pixel basis. It was compared to an earlier algorithm for removing space-varying haze and found to better preserve subtle detail in the image and spectral balance between bands. Future work will concentrate on testing the algorithm as part of a land cover classification system in order to assess its effect on classification accuracy, and on methods for determining when and where in an image it should be applied.

References

CRANE, R. B., 1971, Preprocessing techniques to reduce atmospheric and sensor variability in multispectral scanner data. *Proceedings 7th International Symposium on Remote Sensing of Environment*, p. 1345 (Univ. Michigan: Ann Arbor).

CRIPPEN, R. E., 1987, The regression intersection method of adjusting image data for band ratioing. *International Journal of Remote Sensing*, **8**, 137–155.

CRIST, E. P., and CICONE, R. C., 1984, A physically-based transformation of thematic mapper data—The TM tasselled cap. *IEEE Transactions Geoscience and Remote Sensing*, **22**, 256–263.

CRIST, E. P., LAURIN, R., and CICONE, R. C., 1986, Vegetation and soils information contained in transformed Thematic Mapper data. *Proceedings IGARSS* (ESA, ESTEC, Noordwijk: The Netherlands), pp. 1465–1470.

LAVREAU, J., 1991, De-hazing Landsat Thematic Mapper images. *Photogrammetric Engineering and Remote Sensing*, **57**, 1297–1302.

PAPOULIS, A., 1965, *Probability, Random Variables and Stochastic Processes* (McGraw-Hill: New York).

POTTER, J. F., and. MENDLOWITZ, M. A., 1975, On the determination of haze levels from Landsat data. *Proceedings 10th International Symposium on Remote Sensing of Environment*, p. 695 (Univ. Michigan: Ann Arbor).

SCHANDA, E., 1986, *Physical Fundamentals of Remote Sensing* (Berlin: Springer-Verlag).

SJOBERG, R. W., and HORN, B. K. P., 1983, Atmospheric effects in satellite imaging of mountainous terrain. *Applied Optics*, **22**, 1702–1716.